

# Static and Dynamic Disorder in Topological Systems: Localized, Critical and Extended States

T. ČADEŽ<sup>a,\*</sup>, R. MONDAINI<sup>a</sup>, E.V. CASTRO<sup>b,c,a</sup> AND P.D. SACRAMENTO<sup>c,a</sup>

<sup>a</sup>Beijing Computational Science Research Center, Beijing, 100193, China

<sup>b</sup>Departamento de Física, Universidade do Porto, Porto, Portugal

<sup>c</sup>CeFEMA, Instituto Superior Técnico, Universidade de Lisboa, Av. Rovisco Pais, 1049-001 Lisboa, Portugal

Topological properties may be induced or changed by the action of disorder. We investigate two examples of this scenario: in the first, by showing that either trivial or topological two-dimensional superconductors, as a result of a static random distribution of magnetic impurities, display topological phases. The second one involves using time-dependent perturbations, which also have the general effect of inducing topology and, under appropriate conditions, the appearance of topological properties is shown. In this case, we consider the effect on the topology of one-dimensional systems, of time periodic or aperiodic perturbations consisting of kicks of spatially non-homogeneous potentials. One finds different regimes characterized by localized, critical, or extended non-equilibrium states, as a result of the time dependent perturbation. We further carry out the existence and characterization of the topological edge states that occur both in the case of a static and dynamic perturbations. In the case of the static disorder, the topological phases are characterized calculating the real space Chern number and various regimes for the low energy density of states are identified and explained in the context of general properties of the symmetry classes  $D$  and  $C$ . In the case of a time periodic perturbation (the Floquet regime) we contrast the dynamical localization, and its properties, when using kicks either in the quasiperiodic spatially inhomogeneous potentials of the Aubry–André type or in the case of kicks on the pairing amplitude in the presence of static Aubry–André quasi-disorder. In both, we make use of lattice sizes drawn from the Fibonacci sequence. We also show that aperiodicity in the sequence of time perturbations leads in general to delocalization, a regime characterized by a fully random matrix Hamiltonian with the appropriate symmetry.

DOI: [10.12693/APhysPolA.135.1180](https://doi.org/10.12693/APhysPolA.135.1180)

PACS/topics: topological transitions, Chern numbers, majorana modes, critical states, localization, dynamical localization

## 1. Introduction

Even though topological phases are robust against weak disorder, strong disorder in general induces localization of wave functions [1, 2]. Localized wave-functions are not expected to contribute to the non-trivial topology, so the fate of the topological phase in the presence of strong disorder has attracted interest [3–9]. Naively one would expect that increasing disorder leads to complete electronic localization and trivial topology. Interestingly enough, in certain circumstances the effect of strong disorder may enhance and even stabilize non-trivial topological phases [8–10].

In the case of trivial topology, the effects of static disorder have been classified according to the time reversal symmetry (TRS), spin rotation, and the space dimensionality  $d$  [1, 11, 12]. If the discrete particle–hole and chiral (sublattice) symmetries are absent, then the three Wigner–Dyson classes emerge [1]: unitary (or class-A), for TRS broken systems, irrespectively of spin rotation; symplectic (or class-AII), for TRS preserving systems without spin rotation invariance; orthogonal (or class-AI), for systems which preserve both TRS and spin rotation symmetries. For  $d = 1$ , all states are exponentially

localized for any finite disorder (except for special cases where disorder is spatially correlated, such as the quasi-random Aubry–André potential [13]); for  $d=3$ , a region of extended states exists, separated from localized states by a mobility edge which moves with disorder strength, thus leading to the Anderson localization transition when the mobility edge crosses the Fermi level [14]. In the case of two-dimensional systems in the orthogonal class, several results show that the spectrum is composed only of localized states [15–17]. For symplectic systems, there is an Anderson localization transition, with regions of extended states occurring in the spectrum [3, 16, 18, 19]. In the case of the unitary class, such as in the quantum Hall effect, it was established that at the center of each Landau level band there is one critical state — an extended state where the localization length diverges linearly with system size [17, 20]. This holds in the unitary class when spin rotation is conserved. In the case when both TRS and spin rotation symmetry are broken, the physics was found to be different [4–7]. It seems well established that a band of extended states, and not a single state, shows up. Depending on the model, this band can be made entirely of critical states, or can be a band of truly extended states. Interestingly enough, when the band is made of critical states, the transition to the localized phase at the critical energy is accompanied by a divergent localization length reminiscent of a Berezinskii–Kosterlitz–Thouless transition [21]. A one-dimensional system with a quasi-random potential displays regimes with the various types

\*corresponding author; e-mail: [tilen.cadez@csrc.ac.cn](mailto:tilen.cadez@csrc.ac.cn)

of states, as a function of the amplitude of the potential term. For small amplitudes, they are extended. Beyond a certain amplitude, the states become localized and at the transition point, they acquire a fractal nature, revealing its critical behavior, in an intermediate regime between the fully extended and the localized states [13].

Localization due to disorder may also be obtained dynamically. Specifically, for the case of a system with delocalized states, it has been shown that imposing a time dependent spatially non-homogeneous perturbation, may lead to dynamical localization of the states under appropriate conditions. For example, a periodic time-dependent fully random potential leads to localization in one-dimensional systems. On the other hand, a time-periodic perturbation with a non-homogeneous quasi-random potential, as the Aubry–André potential, leads to regimes of extended, localized, and critical states [22]. The time-evolution operator describing the dynamics of a time-periodic Hamiltonian at stroboscopic times,  $\hat{H}(t+T) = \hat{H}(t)$ , is captured by  $\hat{U}(nT) = e^{-i\hat{H}_{\text{eff}}nT}$ , where  $\hat{H}_{\text{eff}}$  is a time-independent Hamiltonian, often referred to as the Floquet Hamiltonian. Following one period, the time-evolution operator can be written in terms of its eigenstates  $|\theta_m\rangle$  and the quasi-energies  $\varepsilon_m$ , connected to its actual eigenvalues, as  $\hat{U}(T) = e^{-i\hat{H}_{\text{eff}}T} = \sum_m e^{-i\varepsilon_m T} |\theta_m\rangle \langle \theta_m|$ .<sup>†</sup>

A closed form of the effective Floquet Hamiltonian is not always obtainable, i.e., is not always possible to find an effective time-independent Hamiltonian, written in terms of local operators that would be sufficient to describe the stroboscopic dynamics of the system. This caveat is connected to the convergence of the Magnus expansion, often employed to obtain  $\hat{H}_{\text{eff}}$  in the high-frequency regime ( $T \ll 1$ ). Considering a driving protocol that is time-symmetric, i.e.,  $\hat{H}(t) = \hat{H}(T-t)$ , the time evolution operator can be written as  $\hat{U}(T) = e^{i\lambda\hat{V}/2} e^{-i\hat{H}_0 T} e^{i\lambda\hat{V}/2}$ , with  $\hat{H}_0$  the time independent Hamiltonian and  $\hat{V}$  the time dependent perturbation, with amplitude  $\lambda$ . Using this simple form, one can explicitly construct the Floquet Hamiltonian by making use of the analogue of the Baker–Campbell–Hausdorff (BCH) formula applied to time symmetric problems [23],  $\exp \hat{Y} \exp \hat{X} \exp \hat{Y} = \exp(\hat{X} + 2\hat{Y} - \frac{1}{6}[[\hat{X}, \hat{Y}], \hat{Y}] + \frac{1}{6}[\hat{X}, [\hat{X}, \hat{Y}]] + \dots)$ , as

$$\begin{aligned} \hat{H}_{\text{eff}} &= \hat{H}_0 + \frac{\lambda}{T} \hat{V} - \frac{T\lambda}{12} [\hat{H}_0, [\hat{H}_0, \hat{V}]] \\ &+ \frac{\lambda^2}{24} [[\hat{H}_0, \hat{V}], \hat{V}] + \dots \end{aligned} \quad (1)$$

<sup>†</sup>We note that there is an ambiguity in the definition of the effective Hamiltonian since the Floquet quasi-energies can be shifted by a multiple of  $\omega = 2\pi/T$ . The quasi-energy Floquet first Brillouin zone is thus between  $-\omega/2$  and  $\omega/2$  and  $\varepsilon_m T$  is between  $-\pi$  and  $\pi$

In the limits of high-frequency ( $T \ll 1$ ) and small kick-amplitudes ( $\lambda \ll 1$ ), one can truncate the effective Hamiltonian in the first order as

$$\hat{H}_{\text{eff}} = \hat{H}_0 + \frac{\lambda}{T} \hat{V}. \quad (2)$$

Such expansion tells us that the small period regime is equivalent to the static problem, with an appropriately renormalized potential, and therefore the high frequency regime is related to the static problem.

As an example, a simple tight-binding model perturbed by either Anderson disorder or a Aubry–André like potential was considered before [22]. The Aubry–André potential is written as a local chemical potential of the form  $\mu_i = \lambda_1 \cos(2\pi\alpha i + \varphi)$ , where  $\alpha$  is an irrational number, and therefore the potential is incommensurate with the lattice. A usual choice is  $\alpha = (\sqrt{5}-1)/2$ , the inverse golden ratio. Here we use  $\alpha = \alpha_n$ , where  $\alpha_n = F_{n-1}/F_n$  and  $F_n$  are the Fibonacci numbers, which are defined recursively as  $F_n = F_{n-1} + F_{n-2}$ , with  $F_1 = F_2 = 1$ . Taking the  $\lim_{n \rightarrow \infty} \alpha_n$  one gets  $(\sqrt{5}-1)/2$ , i.e., an inverse of the golden mean. For the case of periodic (open) boundary conditions one takes for system size  $L = F_n$  ( $L = F_n + 1$ ) and with  $\alpha_n$  the chemical potential becomes periodic with period  $L$ . One can, therefore, simulate the effect of an Aubry–André quasiperiodic (or quasirandom) potential, considering a sequence of the Fibonacci sizes and taking  $\alpha = \alpha_n$ , as above.

Perturbing periodically with a period  $T$  the tight-binding model with hopping amplitude  $w$ , leads to a set of eigenstates that in the small period regime, or high frequencies, display the behavior expected of the static problem with a potential amplitude scaled by  $T$  (see Eq. (2)). For general period and potential amplitude  $\lambda$ , the description requires a diagonalization of the time-evolution operator over a period (the Floquet operator). The states may be characterized in each regime in different ways. One possible way is to calculate the participation ratio (PR) of the eigenstates or its mean value over all eigenstates. The participation ratio for a given eigenstate labelled by  $m$  is defined as  $\mathcal{R}_m = 1/\sum_i |\theta_i^m|^4$ . The average PR,  $\overline{\mathcal{R}} = \langle 1/\sum_i |\theta_i^m|^4 \rangle_{m,r}$ , may be calculated as a function of  $\lambda$  and  $T$ . Here,  $\langle \cdot \rangle_{m,r}$  denotes first the average over all the eigenstates  $|\theta^m\rangle = \sum_i \theta_i^m |i\rangle$  in the site basis  $|i\rangle$ , which are then averaged over different realizations  $r$ , where different realizations consist of different choices of  $\varphi$ 's. The average PR quantifies the average spreading of the eigenvectors in real space. In the absence of the potential ( $\lambda = 0$ ), all  $|\theta^m\rangle$  are plane waves, for which  $\overline{\mathcal{R}} = L$  and for general delocalized states  $\overline{\mathcal{R}} \sim \mathcal{O}(L)$ , whereas for perfectly localized states  $\overline{\mathcal{R}} = 1$ . In Fig. 1, we show the results for the average normalized participation ratio (NPR) for a tight-binding model, in a system with 145 sites. In the low period and small amplitude regime one finds the transition from the extended states, with large  $\overline{\mathcal{R}}/L$ , and the localized states, with corresponding small  $\overline{\mathcal{R}}/L$ . The transition line between the two regimes extends to finite values of  $T$  and  $\lambda$ , and is characterized by critical states, as in the

case of the static Aubry–André model. For larger values there is a crossover between the extended and localized states, whose proper interpretation in terms of a static Hamiltonian would require the inclusion of higher order terms, as the extra ones shown in the right-hand side of Eq. (1). Using lattices whose sizes are obtained from the Fibonacci sequence, qualitatively captures well the main results obtained for much larger lattices [22], and even for fairly small system sizes. For that reason we will also use  $L$ 's chosen from the Fibonacci sequence, when investigating the kicked Kitaev model, in Sect. 3.

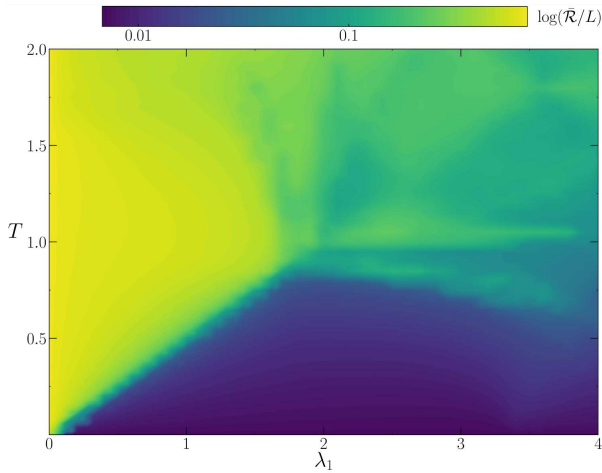


Fig. 1. Phase diagram of the periodically kicked tight-binding model, showing the normalized participation ratio as a function of the period and kick amplitudes,  $T$  and  $\lambda_1$ , respectively. The kicks consist of instantaneous quenched potentials of the form  $\mu_i = \lambda_1 \cos(2\pi\alpha_n i + \varphi)$ , with  $\alpha_n = F_{n-1}/F_n$ , a ratio of two consecutive Fibonacci numbers, for a system of  $L = F_{12} + 1 = 145$  sites.

For topological systems a new class of localized states arises, the edge states, that are robust under weak disorder, provided some discrete symmetries are preserved [24, 25]. The interplay of topology and localization was first analyzed in the context of the robustness under disorder of the Hall conductivity quantization, in the integer quantum Hall effect [26]. This is an example of a Chern insulator that belongs to the symmetry class A (all discrete symmetries are broken) in the standard classification. For moderate disorder, the states in the edges of the conduction and valence bands start to localize. As disorder increases, the gap is totally populated by localized states and the extended states carrying the Chern number, the topological invariant that characterizes these topological phases, shift towards one another and annihilate, leading to the topological phase transition. As mentioned above, the difference between the two classes is that, while in the symplectic class AII, a finite region of extended states with a well defined mobility edge remains until the transition takes place, there is no mobility edge in the unitary class A systems. The extended states carrying the Chern number are located at particular single energies.

More recently topological states were proposed as a result of a set of (classical) magnetic impurities on top of a conventional superconductor with their spin orientations arranged in some helical way [27, 28]. A chain of magnetic adatoms, ferromagnetically arranged in the presence of spin–orbit coupling and placed on top of a two-dimensional conventional superconductor, led to similar results [29] and localized zero energy modes were detected at the edges of adatom chain using STM: being a superconductor, these edge states were interpreted as the Majorana zero energy modes (MZEM) [30]. Other configurations of magnetic impurities such as different chains or islands [27–29, 31–53] also lead to topological properties [54–56]. If the magnetic impurities have arbitrary orientations and locations, the pair breaking effect leads to gapless superconductivity and eventually destruction of superconductivity occurs for small concentration of impurities of the order of a few percent [57]. However, a higher robustness of superconductivity to the increasing number of magnetic impurities has been found if they are correlated, particularly if their locations are not random but organized in some patterns [58]. Several works show that regularly positioned chains of adatoms give rise to MZEM such as the cases of random, spiral AFM and FM orientational orderings of the magnetic adatoms. Here we consider the effect of random positional distributions of magnetic impurities with correlated orientations on a conventional superconductor with spin–orbit coupling and show that topological properties are also induced. On the other hand, triplet superconductors are topological in the absence of impurities. Several two-dimensional superconductors also have topological properties such as the so-called  $p+ip$  pairing [59, 60]. Adding spin–orbit interaction and a magnetic field either through its Zeeman effect or due to the presence of vortices, a great variety of topological phases are predicted [61]. Since both a triplet superconductor and a magnetic chain induce topological states, one may explore the combined effect of the two by considering a set of magnetic impurities on top of a triplet superconductor [41, 62]. It is also shown here that the topology may be changed by adding magnetic impurities, distributed randomly [63].

## 2. Effects of disorder in $Z$ class superconductors

A single magnetic impurity in a conventional superconductor coupled to the conduction electron spin density gives rise to a local bound state, known as the Yu–Shiba–Rusinov (YSR) state [64–70]. As the exchange coupling  $J$  between the impurity and the electron spin density increases, a first order quantum phase transition (QPT) occurs [71–73], at which point the gap function has a  $\pi$  shift and the magnetization of the conduction electrons jumps from zero to  $1/2$ . The YSR states come in pairs that lay inside the gap (one at positive and one at negative energy) and tend to lower energies as the coupling grows. At the quantum critical point there is a level crossing, such that the bound state has a small but finite energy.

Increasing the number of impurities, more states appear inside the gap (two per impurity) and as the coupling increases, a series of quantum phase transitions occurs and the magnetization of the conduction electrons changes in increasing plateaus. If the number of magnetic impurities is large enough there are bound states inside the gap that have zero energy and constitute self-conjugate Majorana fermions. It has been shown that the quantum phase transition that results from the closing of the gap as a function of the coupling between the local impurities and the conduction electron spin density coincides with the topological transition to a topological phase with the Majorana fermions [51].

In the superconducting systems there are four symmetry classes [74]: superconductors with  $s$ -wave pairing symmetry with a particle-hole symmetry corresponding to a spin singlet where the operator squares to  $-1$  are characterized by a  $C$  class where time-reversal symmetry is broken or a  $CI$  class where time-reversal symmetry is present and squares to  $+1$ . There are also superconductors with  $p$ -wave symmetry of the class  $D$  where time-reversal symmetry is broken, and with preserved time-reversal symmetry, class  $DIII$ , where the time-reversal operator squares to  $-1$ . In two dimensions both time-reversal symmetry breaking classes,  $D$  and  $C$ , may be characterized by a  $Z$  topological invariant. In the case of time-reversal symmetry the  $p$ -wave superconductor, class  $DIII$ , is characterized by a  $Z_2$  topological invariant, while the  $s$ -wave superconductor,  $CI$  class is topologically trivial. Adding magnetic impurities to a superconductor breaks time-reversal symmetry and therefore one expects for both types of pairing symmetries a class  $Z$  superconductor. The 1D Kitaev model that we will consider ahead, belongs to the BDI class, which is also a class  $Z$  superconductor.

In order to study the effect of magnetic impurities we introduce a two-dimensional superconductor with spin-orbit interaction in the presence of a uniform magnetic field [61]. Spinfull electrons in the presence of a Zeeman term (that breaks TRS) and in the presence of the Rashba spin-orbit coupling are in a superconducting state with both singlet and triplet pairing symmetry (parity is broken due to the presence of the spin-orbit coupling). The Hamiltonian  $\hat{H} = \hat{H}_0 + \hat{H}_\Delta$  is given by the sum of various terms,  $\hat{H}_0 = \epsilon_{\mathbf{k}}\sigma_0 - h_z\sigma_z + \hat{H}_R$ . Here,  $\epsilon_{\mathbf{k}} = -2w(\cos k_x + \cos k_y) - \mu$  is the kinetic part,  $w$  denotes the hopping parameter set in the following as the energy scale,  $\mu$  is the chemical potential,  $\mathbf{k}$  is a wave vector in the  $xy$  plane, and we have taken the lattice constant to be unity. The Zeeman splitting  $h_z$  is responsible for the magnetization and  $\hat{H}_R$  is the Rashba spin-orbit term,  $\hat{H}_R = \mathbf{s} \cdot \boldsymbol{\sigma} = \alpha_R (\sin k_y \sigma_x - \sin k_x \sigma_y)$  where  $\alpha_R$  is measured in the energy units and  $\mathbf{s} = (\sin k_y, -\sin k_x, 0)$ . The vector  $\boldsymbol{\sigma} = (\sigma_x, \sigma_y, \sigma_z)$  is the vector of the Pauli matrices acting on the spin sector and  $\sigma_0$  is the  $2 \times 2$  identity. The pairing matrix reads  $\hat{\Delta} = i(\mathbf{d} \cdot \boldsymbol{\sigma} + \Delta_s)\sigma_y$ . The system has a rich phase diagram with trivial and topological phases. These are shown in Fig. 2 considering

$d_z = 0, \Delta_s = 0$  and choosing  $d_x = \Delta_t \sin k_y, d_y = -\Delta_t \sin k_x$ . The lines in the phase diagram correspond to the gapless points that separate the different topological phases. The superconductor we consider here is time-reversal invariant if the Zeeman term is absent (it is not of the  $p + ip$  type). The system then belongs to the symmetry class  $DIII$  where the topological invariant is a  $Z_2$  index. If the Zeeman term is finite, TRS is broken and the system belongs to the symmetry class  $D$ . The topological invariant that characterizes this phase is the first Chern number  $C$ . If  $h_z = 0$  and the pairing is  $s$ -wave, the system is in a topologically trivial phase: there is only the bulk gap and no gapless (edge) states. In the case of  $p$ -wave or when there is a mixture of  $s$ - and  $p$ -wave components, and the amplitude of the  $p$ -wave pairing is larger than the corresponding amplitude of the  $s$ -wave case, there are two counter-propagating edge modes that give opposite contributions to the total Chern number,  $C = 0$  ( $Z_2$  phase). As the Zeeman term is turned on, TRS is broken. For small magnetization, the superconductor is in a trivial phase with the Chern number  $C = 0$ . A finite magnetization causes a topological phase transition to a phase with non-zero Chern number. This happens both for the  $p$ -wave case and the  $s$ -wave case.

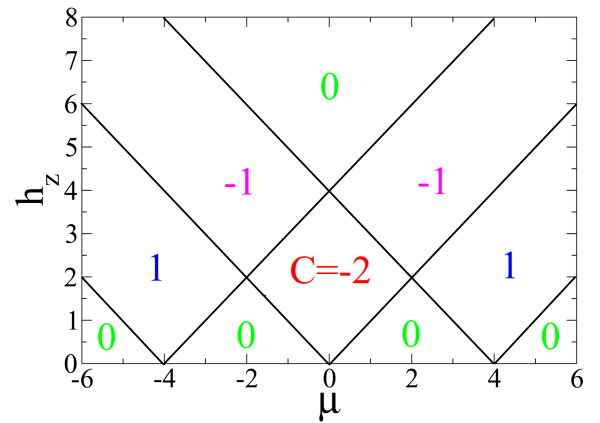


Fig. 2. Phase diagram of a triplet superconductor as a function of chemical potential and the Zeeman splitting.  $C$  is the Chern number. In the case of a singlet superconductor the phase diagram is similar, particularly at finite  $h_z$ . Without the Zeeman term, however, the system is topologically trivial.

In this section we consider the possibility of inducing topological order as a result of adding orientationally correlated magnetic impurities, in growing concentrations,  $c_i$ , and distributed randomly in over  $c_i N$  sites of the underlying  $N$ -sites square lattice ( $c = 1$  is the uniform field case). The impurities act as local Zeeman fields, aligned along the  $z$ -direction. The average over disorder is obtained over 100 impurity configurations. Considering that at half-filling ( $\mu = 0$ ) any infinitesimal uniform field induces chiral modes on the edges of the two-dimensional system (see Fig. 2), one may expect that a finite concentration of magnetic impurities may induce chiral edge modes and non-trivial topology.

The topological invariant Chern number is naturally defined in case the system is translationally invariant. Introducing disorder will break this invariance. Imposing twisted boundary conditions we may generalize the definition of the Chern number considering a circulation over the boundary conditions instead of over the edges of the Brillouin zone [26, 62, 75, 76]. In Fig. 3 we show results for the real-space Chern number for two cuts, one at  $\mu = 0$  and the other at  $\mu = -3$ , as a function of impurity concentration,  $c_i$ , and for different amplitudes of the local Zeeman field,  $h_z$ . Due to disorder averaging the Chern number is not necessarily an integer (even though it is an integer for each disorder configuration). Nevertheless, a topological phase is characterized by an integer Chern number. For high impurity concentrations the results are qualitatively similar to those of the uniform Zeeman field shown in Fig. 2. The results clearly show the appearance or change of topological regimes due to the effect of the TRS breaking that results from the introduction of the random magnetic impurities.

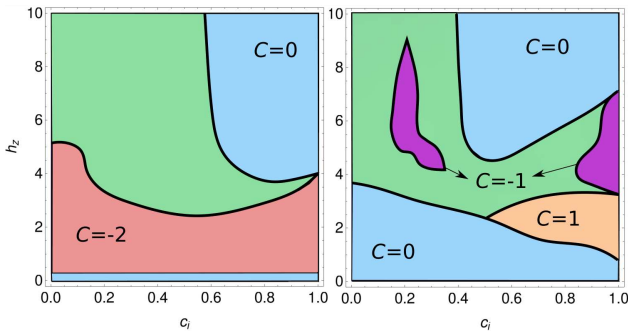


Fig. 3. The Chern number for a triplet superconductor for  $\mu = 0$  (left) and  $\mu = -3$  (right) for different impurity concentrations,  $c_i$ , and different Zeeman field amplitudes,  $h_z$ . The green region stands for a thermal metal regime, where the Chern number is not quantized.

In the case of uniform field the spectrum is usually gapped, with the exception of the transition lines shown in Fig. 2 where the spectrum becomes gapless. The level structure is however different if there is disorder, and states inside the gap appear and typically grow in number as disorder increases. This behavior is reflected in the density of states (DOS).

The DOS is obtained by numerically diagonalizing the Bogoliubov–de Gennes (BdG) equations for a finite system, of size  $21 \times 21$  or using the recursive Green function method which allows larger system sizes.

In Fig. 4, top parts, we illustrate the behavior of the DOS for the case of an  $s$ -wave superconductor with chemical potential  $\mu = 0$ . In the left-top part we consider  $h_z = 4$  and change the concentration, and in the right-top part we fix  $c_i = 0.3$  and change  $h_z$ . In both cases, increasing  $c_i$  or  $h_z$ , increases the disorder. The gap gets filled with states, and the density of states at low energies increases and is finite at zero energy. Even though the gap gets filled, the coherence peaks at the gap lo-

cation remain clear, even though for large concentrations they are less sharp. This is similar to the result obtained for a random distributions of vortices but in this case the density of states at low energies behaves as  $\rho(E) \sim E^a$ , where the exponent  $a$  depends on the vortex concentration [77]. With increasing concentrations or increasing  $h_z$  the zero energy peak decreases since one is approaching a regime where a gap with magnetic origin appears.

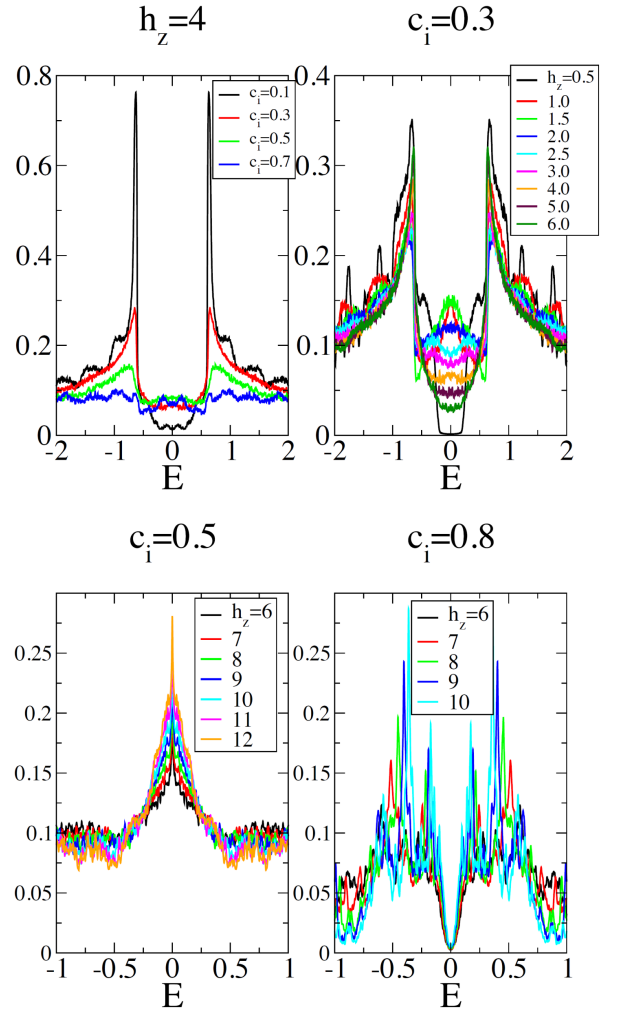


Fig. 4. Density of states for a  $s$ -wave superconductor (top parts) and a  $p$ -wave superconductor (bottom parts) with magnetic impurities.

The case of the  $p$ -wave triplet superconductivity with chemical potential  $\mu = 0$  is shown in Fig. 4, bottom parts. Small values of  $\rho(E = 0)$  correspond to gapped regions that are seen for small concentrations and small values of  $h_z$ . As disorder increases, the density of states increases inside the gap (as in the  $s$ -wave case). After the gap closes, and there is a transition to a thermal metal regime, the density of states at zero energy has a zero value, which grows to a finite value and a sharp peak that increases with disorder, if the concentration is not too large. This behavior is characteristic of a disordered

$D$  class superconductor [78, 79]. It signals the presence of a thermal metal and corresponds to the green region in the phase diagrams of Fig. 3. In the thermal metal regime the system is gapless and only the thermal Hall conductance is quantized. At the transition where the density of states is supposed to vanish like  $\rho(E) \sim |E| \log |E|$ , one expects the presence of critical states, intermediate between extended and localized states. Close to  $c_i = 1$ , however, the zero energy peak decreases. This is particularly visible for  $\mu = 0$  (for  $h_z \leq 5$ ). As can be seen from Fig. 2, one enters a trivial gapped regime in the uniform case. A growing zero energy DOS peak characteristic of the thermal metal regime is seen for  $c_i = 0.5$ . For  $c_i = 0.8$  we see that, contrarily, the density of states has a dip at zero energy, as mentioned above.

### 3. Effects of dynamic disorder on 1d Kitaev model

After studying the effects of static disorder, in this section we focus on the dynamic disorder in topological systems. For this, we consider the time-dependent Hamiltonian

$$\hat{H}(t) = \hat{H}_{0w} + \hat{H}_{0\Delta} + \hat{H}_{0\mu} + \hat{H}_{1\Delta}(t) + \hat{H}_{1\mu}(t), \quad (3)$$

where  $\hat{H}_{0w} = -\sum_i (w \hat{c}_i^\dagger \hat{c}_{i+1} + \text{H.c.})$  is the kinetic energy,  $\hat{H}_{0\Delta} = -\sum_i (\Delta_0 \hat{c}_i^\dagger \hat{c}_{i+1}^\dagger + \text{H.c.})$  is the superconducting  $p$ -wave pairing and  $\hat{H}_{0\mu} = -\sum_i \mu_{0i} \hat{c}_i^\dagger \hat{c}_i$  is the chemical potential, and H.c. stands for the Hermitian conjugate of the preceding terms. The fermionic creation (annihilation) operator at site  $i$  is  $\hat{c}_i^\dagger$  ( $\hat{c}_i$ );  $w$  and  $\Delta_0$  are the homogeneous hopping and superconducting  $p$ -wave pairing between neighboring sites, respectively. The fourth term in the Hamiltonian  $\hat{H}_{1\Delta} = -\sum_\tau \delta(t - t_\tau) \sum_i (\Delta_1 \hat{c}_i^\dagger \hat{c}_{i+1}^\dagger + \text{H.c.})$  are the kicks in spatially homogeneous  $p$ -wave pairing and finally the last term is  $\hat{H}_{1\mu} = -\sum_\tau \delta(t - t_\tau) \mu_{1i} \hat{c}_i^\dagger \hat{c}_i$ . The inhomogeneous chemical potentials are  $\mu_{bi} = \mu_b + \lambda_b \cos(2\pi\alpha_n i + \varphi)$ , with  $b = 0, 1$  and  $\alpha_n = F_{n-1}/F_n$  as specified in Introduction<sup>‡</sup>. The last two terms in the Hamiltonian are applied onto the system at times  $t_\tau$  and the integer  $\tau$  counts the number of applied kicks. Note that we either consider kicks in quasiperiodic chemical potential (thus setting  $\Delta_1 = \mu_1 = \lambda_0 = 0$  and we mostly focus on  $\mu_0 = 0$ ) or we consider kicks in homogeneous pairing  $\Delta_1$  (by taking  $\Delta_0 = \mu_0 = \mu_1 = 0$  and  $\lambda_1 = 0$ ).

The unperturbed Hamiltonian,  $\hat{H}_0 = \hat{H}_{0w} + \hat{H}_{0\Delta} + \hat{H}_{0\mu}$ , is for constant  $\mu_{0i} = \mu_0$  the 1D Kitaev model [80]. When  $|\mu_0| < 2w$  the system is in a topological phase

with non-vanishing winding number (if  $\Delta_0 \neq 0$ ) and if  $|\mu_0| > 2w$  the system is topologically trivial. At  $|\mu_0| = 2w$  the system is gapless as well as when  $\Delta_0 = 0$ . This line separates two topological phases, whereas  $|\mu_0| = 2w$  separates the topological phases from the trivial regimes. In the topological phases, if the system is finite, there are edge Majorana modes, that decay exponentially from the edge towards the bulk of the chain. When  $\Delta_0 = w$  the edge states are perfectly localized at the edge. In a translational invariant system the single-particle states at  $\Delta_0 = w$  have a dispersionless flat band (FB) with energy  $2w$ .

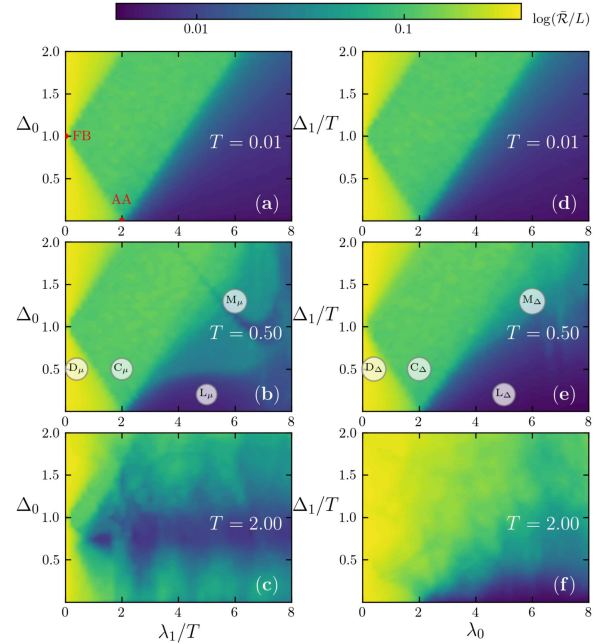


Fig. 5. Comparison of the phase diagrams of spinless fermions for the two types of periodic kicks as quantified by the NPR for kicks in chemical potential  $\lambda$  (parts a–c)) and in pairing  $\Delta$  (parts d–f)) for low ( $T = 0.01$ , parts a,d), intermediate ( $T = 0.5$ , parts b, e) and high period ( $T = 2$ , parts c, f) regimes. The system size was  $L = F_{12} + 1 = 145$ ,  $\mu_0 = \mu_1 = 0$  and we used 10 disorder realizations.

We report in Fig. 5 the phase diagrams for two types of periodic kicks. In the left column, we consider the Kitaev chain (we set  $w = 1$  as the energy unit) with  $\mu_0 = 0$ ,  $\Delta_0 \neq 0$ ,  $\lambda_0 = 0$ , and take a time-dependent perturbation with  $\lambda_1 \neq 0$  and  $\Delta_1 = 0$ . In the right column, we consider  $\mu_0 = 0$ ,  $\Delta_0 = 0$ ,  $\lambda_0 \neq 0$  and  $\lambda_1 = 0$ ,  $\Delta_1 \neq 0$ . Therefore, in the first column the spatially quasi-periodic potential is due to the time dependent perturbation ( $\lambda_0 = 0$ ,  $\lambda_1 \neq 0$ ), while in the second column the disorder is due to the time independent term ( $\lambda_0 \neq 0$ ,  $\lambda_1 = 0$ ) and the kicks are the result of a time-dependent pairing ( $\Delta_0 = 0$ ,  $\Delta_1 \neq 0$ ). The phase diagrams are parametrized by the average NPR, as shown in Fig. 1. In part Fig. 5a we also denote two special points, the FB point with a dispersionless flat band and the duality point AA, which denotes the metal–insulator transition point in the absence of pairing.

<sup>‡</sup>We note that by taking either rational approximation or irrational value of  $\alpha$  makes no difference when it comes to either the bulk properties or the number of Majorana edge states. The difference, however is in the number of normal fermionic — Andreev edge states, in the case of irrational  $\alpha$  value there are typically a few more such states present for comparable system sizes

For small periods,  $T = 0.01$  (high frequency), the phase diagram is qualitatively the result for a static problem with a renormalized  $\lambda_1/T$  in the first case and  $\Delta_1/T$  in the second case. As in the case of Fig. 1 the lighter color regimes correspond to extended states and then there is a transition to a regime of critical states and another transition to a regime of localized states. In this model the regime of critical states is of finite extent, in contrast to the transition line found in the problem with no pairing. The localized nature of the flat band part clearly determines that close to  $\Delta_0 = 1$  (or  $\Delta_1/T = 1$ , even though since in this case  $\Delta_0 = 0$  it cannot be argued straightforwardly that we are perturbing around the flat point) the extended nature of the states for small  $\lambda_1/T$  or  $\lambda_0$  changes to critical states.

As the period  $T$  increases, the zeroth order of the BCH approximation does not hold anymore and a behavior characteristic of the dynamic disorder emerges. At  $\mu_0 = 0$  the region of critical states separates in two regimes with a clear distinction of the average NPRs, at least for intermediate periods, such as  $T = 0.5$  in the case of  $\lambda_1$  kicks (Fig. 5b). For larger periods, the plateau structure smears out. If  $\mu_0 \neq 0$  the change from the delocalized to the localized regime occurs gradually and the plateaus are smeared out. Also, if the kicks are due to pairing ( $\Delta_1 \neq 0, \lambda_1 = 0$ ) the second plateau is less clear.

The nature of the plateaus is better understood by looking at the distribution of NPRs. This is shown in Fig. 6, for points marked in the phase diagram of Figs. 5b and e. A typical extended system has a strongly peaked NPR distribution at values  $\tilde{\mathcal{O}}(1)$ . A point in the first plateau has a distribution peaked at smaller values of NPR, clearly distinguishing it from the extended states, confirming that the critical states have a spatial extension that is intermediate between the extended states and the localized states. These have a distribution peaked at small NPR values. Interestingly, the states in the second plateau have a two-peak distribution of NPRs, with one peak at the critical states range and another at small values of NPR, as the localized states. As Fig. 6 also shows, this is not seen when the kicks are the result of pairing ( $\Delta_1 \neq 0$ ).

To acquire a better understanding on the physical aspects of these different types of states, we report in Fig. 7 the wave functions (or more appropriately the density probabilities) for the points indicated in Fig. 5b, extended ( $D_\mu$ ), critical ( $C_\mu$ ) and localized ( $L_\mu$ ), for the case of potential kicks, as well as their corresponding particle and hole weights,  $u$  and  $v$  in the standard BdG representation. The intermediate nature of the critical states is clearly illustrated.

The response of the system to a periodic perturbation is fully characterized by the Floquet operator  $U(T)$ . In Fig. 8, we compare the NPR of the eigenstates of the Floquet operator in different regimes, selecting the four phases identified, as a function of the quasi-energies. Both cases of potential and pairing kicks are considered. Since we are focusing on the case of  $\mu_0 = 0$  we are

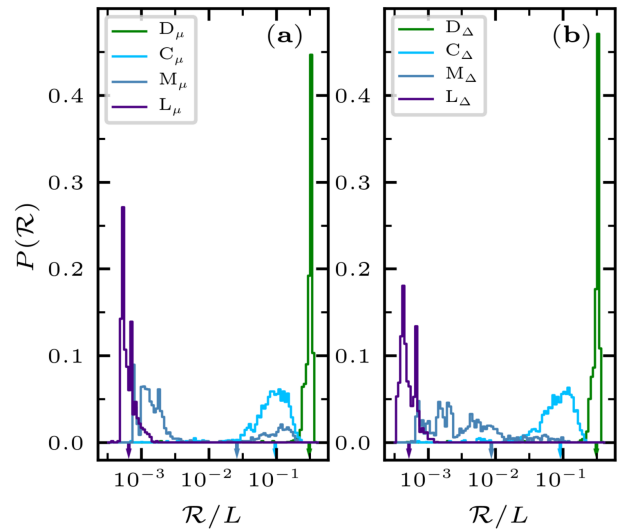


Fig. 6. Distribution of NPR values obtained across the whole eigenstate spectrum for different representative points in the phase diagram with  $T = 0.5$ , as marked in Figs. 5b and e, for both types of kicks we investigate for the system size  $L = F_{17} + 1 = 1598$ .

perturbing the system that is originally in a topological regime. In the unperturbed case, using open boundary conditions, there are the Majorana zero energy edge modes. In the regime of delocalized states the participation ratio scales with the system size, while in the critical regimes it scales as  $L^\beta$ , with  $\beta \sim 0.2$  [81]. In the delocalized regime the zero energy states with a small NPR are clearly seen. Other states with small NPR appear but with finite energy. In the critical regime two types of behavior emerge. In a first case,  $C_\mu$  and  $C_\Delta$  there is some mixture of extended states (even though with smaller NPR values as compared with the regime of the left part) and states that have smaller NPRs. In the second regime of critical states, there is a clear mixture of states with different ranges of NPRs. This is particularly noticeable in the case of potential kicks and there is a separation of both types of states in quasienergy space indicating the appearance of a mobility edge [81]. In the case of pairing kicks, while there are two separate sets of states with large and small NPRs, with the smaller set with values characteristic of localized states, there is no clear quasienergy separation and therefore the mobility edge in the quasienergies is less prominent. This is consistent with the two peak NPR distribution structure of Fig. 6a for the case of potential kicks, while there is a broader distribution seen also in 6b for the pairing kicks and provides further insight into the structure of second plateaus seen in parts in Fig. 5b and e, respectively. In the right parts of Fig. 8 all states have small NPRs characteristic of localized states.

We further consider aperiodic kicks, i.e., by using kicks which are not equally separated in time, aiming in understanding in how robust are the localization properties obtained in the case of periodic kicks.

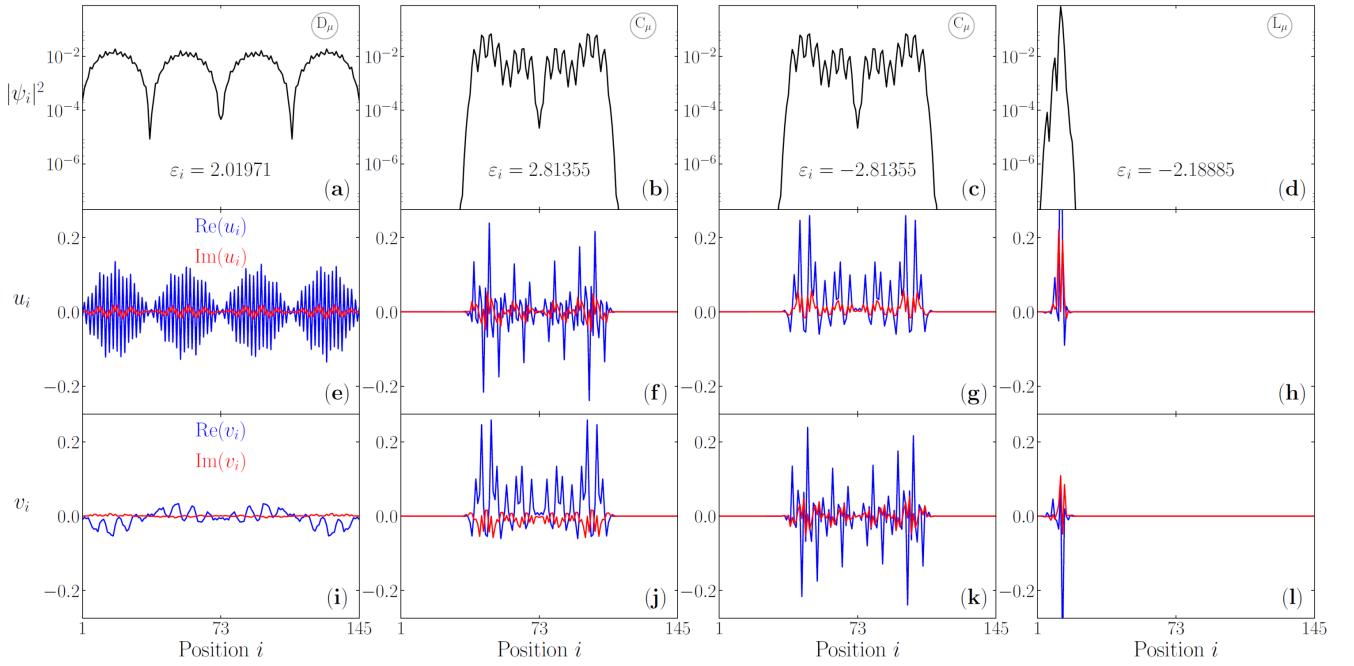


Fig. 7. Examples of delocalized, critical and localized states, for points in the phase diagram defined in Figs. 5b. The two critical states shown in the middle parts are connected via the particle-hole symmetry, i.e., the weights of  $u$  and  $v$  are interchanged and their quasi-energies are symmetric.

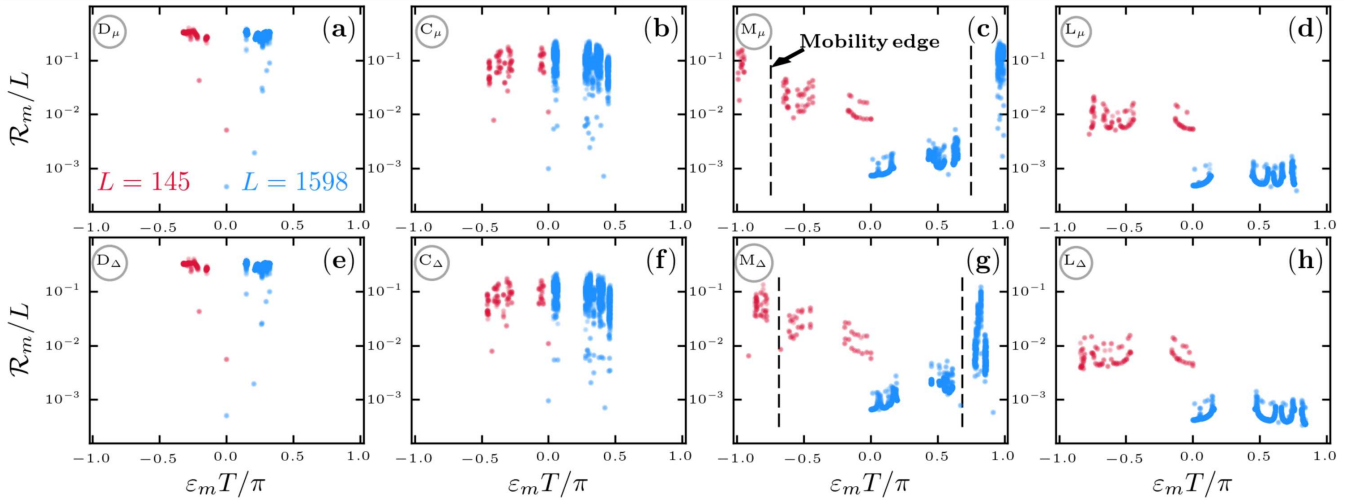


Fig. 8. Normalized participation ratio for each eigenstate of the Floquet operator, using parameters corresponding to different points in the phase diagram (see Fig. 5), due to kicks in the chemical potential and in the pairing. We compare two different lattice sizes,  $L = 145$  and  $1598$ , so as to highlight the extended and localized nature of state states. Only half of the symmetric quasienergy spectrum is shown for each size.

To model that, we assume that the time between two consecutive kicks  $T_\tau$  is a stochastic variable distributed with equal probability between times  $T - \delta t$  and  $T + \delta t$ . Thus, the time of the  $\tau$ -th kick is given as  $t_\tau = t_{\tau-1} + T + \delta t_\tau$ , with  $\delta t_\tau$  being chosen in the interval  $(-\delta t, \delta t)$ , with  $\delta t < T$  so as to obey causality. The time evolution operator after  $\tau$  kicks is, therefore,

$$\hat{U}_\tau = \hat{U}(T_\tau)\hat{U}(T_{\tau-1})\cdots\hat{U}(T_1), \quad (4)$$

with  $T_\tau = t_\tau - t_{\tau-1}$  and  $\hat{U}(T_\tau) = e^{-i\hat{H}_0 T_\tau} e^{-i\lambda\hat{V}}$ . This leads in general to delocalization. We report in Fig. 9 that as the number of kicks  $\tau$  increases, the average NPR converges to a value that is consistent with the value obtained from a fully random matrix with the appropriate symmetry. We compare the case with no superconducting pairing (class  $A$ ) with the cases with pairing (class  $D$ ). Calculating the exponential of a fully random matrix with the symmetry of class  $A$  leads to a set of eigenstates

whose NPR is  $1/2$ . The same exercise for a matrix in class  $D$  leads to an NPR of  $1/3$ . The results show that as a function of the number of kicks  $\tau$ , the results converge to the corresponding asymptotic limits for each class. Since the eigenstates of random matrices are completely delocalized, this indicates that aperiodic kicks cannot sustain the localization we have obtained in the case of periodic kicks before. One may define a scale,  $\tau_c$ , that characterizes the convergence to those limits. For the case of the Aubry–André kicks [22], the characteristic number of kicks  $\tau_c$  is nearly proportional to the system size  $L$ . Besides, the ratio  $\tau_c/L$  displays a power law behavior on the aperiodicity,  $(\tau_c/L) \propto (\delta t/T)^\kappa$ , with  $\kappa \approx -2$ .

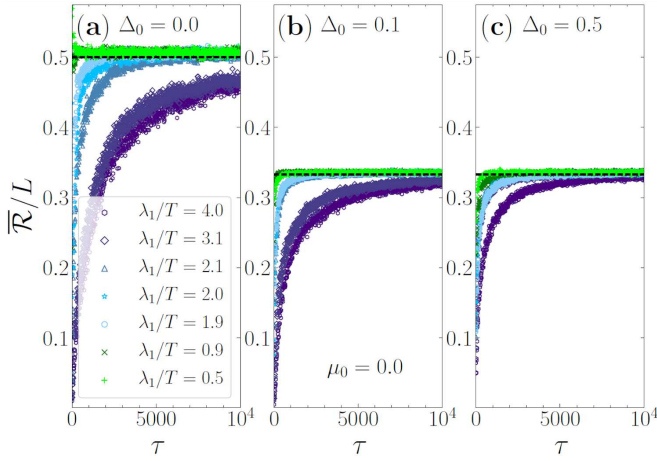


Fig. 9. Stroboscopic evolution of the average normalized participation ratio in the case of aperiodic kicks as a function of the number of kicks. We focus on the case of kicks in the onsite energies with a quasi-periodic fashion, i.e., for  $\lambda_1 \neq 0$ . The lattice size used is  $L = 145$ .

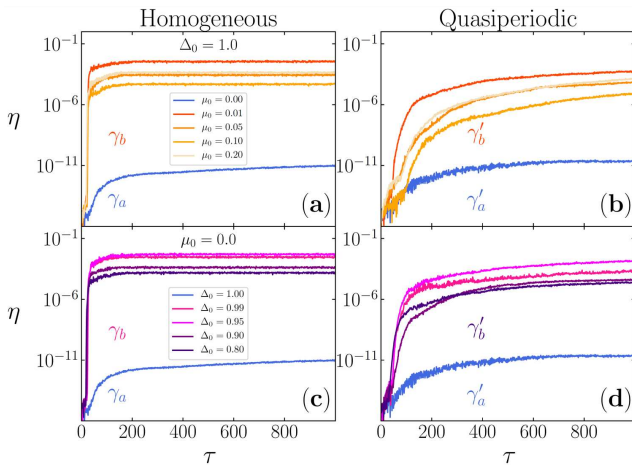


Fig. 10. Evolution of conjugacy of the Majorana modes with either spatially homogeneous kick,  $\mu_1 = 0.2$ ,  $\lambda_1 = 0$  ((a) and (c)) or spatially quasi-periodic kick  $\mu_1 = 0$ ,  $\lambda_1 = 0.2$  ((b) and (d)). We use a small time aperiodicity of  $\delta t = 0.1T$ , the lattice size is  $L = 145$  and  $\lambda_0 = \Delta_1 = 0$ .

Turning back to the case of periodic kicks, we notice that as a result of a periodic time perturbation, edge states may be induced even if the unperturbed system is topologically trivial, in a process often referred to as topological Floquet engineering. In the case of a superconductor these edge states are the Majorana modes. Therefore, in our problem in general there may appear the Majorana modes, either because one starts from a topological regime or due to their appearance as a result of the periodic perturbation. Also, states at the top of the Floquet zone may be induced. Due to the particle–hole symmetry of the BdG equations these states are also Majorana-like but with finite energy,  $\epsilon = \omega/2$ , for a perturbing frequency  $\omega$ . These finite quasienergy Majorana modes are called  $\pi$  Majorana modes, since  $\epsilon_M T = \pi$ . The various Majorana modes are present in the case of delocalized and critical regimes. Its manifestation, however, is masked when the kick period increases since the gaps in the quasienergy spectrum get filled with states. As the NPR analysis shows, if considering regimes in the phase diagram corresponding to either the second plateau or in localized regimes, points  $M$  and  $L$ , respectively, there are various states with small NPR values and the localized nature of the Majorana edge modes is also observed in other states resulting from the effect of disorder. Moreover, edge states (often described as the Andreev bound states) may also appear as a result of the disorder. Although very suggestive, zero quasienergies and small NPR values are not sufficient to characterize a Majorana mode. One may compute [81] the self-conjugacy  $\eta = \sum_i \eta_i$ , with  $\eta_i \equiv ||u_i|^2 - |v_i|^2|$  and  $u_i$  and  $v_i$  being the particle and hole coefficients of the Bogoliubov quasiparticle at site  $i$ . The value of  $\eta$  is vanishing for the Majorana states, ( $\gamma_M = \gamma_M^\dagger$ ), from which follows that  $u_i = v_i^*$ . When the kicks are aperiodic, as studied in various topological systems [81–84], after a few kicks the quasi-energy spectrum in general becomes dense, the gaps are filled with states, and in the system considered in this work the criteria of small energies of NPRs become harder to distinguish the normal fermionic localized states from any surviving Majorana modes. Therefore the self-conjugacy is particularly useful to distinguish between the nature of the two states. This is shown in Fig. 10, where we consider potential kicks, i.e., kicks on the on-site energies with either a homogeneous or a spatially quasi-periodic perturbation, aperiodically in time to study the robustness of the Majorana modes. Also, we consider different types of modes. A Majorana mode  $\gamma_a$  [ $\gamma'_a$ ] is created from the FB point, and multiple Majorana modes  $\gamma_b$  [ $\gamma'_b$ ] from topological regime. Starting from the trivial regime, the Majorana mode is a consequence of the perturbation. Deviating from periodicity the Majorana character is quickly lost [81]. Starting from the flat band point ( $\gamma_a, \gamma'_a$ ) we see that the self-conjugacy remains small as the kicks progress and therefore the Majorana character is preserved approximately. On the other hand, for any other point  $\gamma_b, \gamma'_b$  we see that the self-conjugacy increases with  $\tau$  but even for around 1000 kicks it is still

rather small and considerably smaller than for a normal fermionic mode (of the order of  $10^{-1}-1$ ). In the long time limits, the localized nature of the modes is completely lost, but the perfectly localized Majorana at the flat band point is quite robust, preserving its self-conjugacy.

### Acknowledgments

R.M. was supported by the National Natural Science Foundation of China (NSFC) Grant No. 11674021 and No. 11650110441 as well as NSAF-U1530401. E.C. and P.D.S. acknowledge partial support from FCT through grant UID/CTM/04540/2013. The computations were performed in the Tianhe2-JK cluster at the Beijing Computational Science Research Center (CSRC).

### References

- [1] F. Evers, A.D. Mirlin, *Rev. Mod. Phys.* **80**, 1355 (2008).
- [2] E. Prodan, *J. Phys. A Math. Theor.* **44**, 113001 (2011).
- [3] M. Onoda, Y. Avishai, N. Nagaosa, *Phys. Rev. Lett.* **98**, 076802, (2007).
- [4] Z. Qiao, Y. Han, L. Zhang, K. Wang, X. Deng, H. Jiang, S.A. Yang, J. Wang, Q. Niu, *Phys. Rev. Lett.* **117**, 056802, (2016).
- [5] Y. Su, C. Wang, Y. Avishai, Y. Meir, X.R. Wang, *Sci. Rep.* **6**, 33304 (2016).
- [6] C. Wang, Y. Su, Y. Avishai, Y. Meir, X.R. Wang, *Phys. Rev. Lett.* **114**, 096803, (2015).
- [7] Z. Xu, L. Sheng, D.Y. Xing, E. Prodan, D.N. Sheng, *Phys. Rev. B* **85**, 075115, (2012).
- [8] E.V. Castro, M.P. López-Sancho, M.A.H. Vozmediano, *Phys. Rev. B* **92**, 085410, (2015).
- [9] E.V. Castro, R.D. Gail, M.P. López-Sancho, M.A.H. Vozmediano, *Phys. Rev. B* **93**, 245414, (2016).
- [10] J. Li, R.L. Chu, J.K. Jain, S.Q. Shen, *Phys. Rev. Lett.* **102**, 136806 (2009).
- [11] A. Altland, M.R. Zirnbauer, *Phys. Rev. B* **55**, 1142, (1997).
- [12] B. Kramer, A. MacKinnon, *Rep. Prog. Phys.* **56**, 1469 (1993).
- [13] S. Aubry, G. André, *Ann. Israel Phys. Soc.* **3**, 18 (1980).
- [14] P.W. Anderson, *Phys. Rev.* **109**, 1492 (1958).
- [15] E. Abrahams, P.W. Anderson, D.C. Licciardello, T.V. Ramakrishnan, *Phys. Rev. Lett.* **42**, 673 (1979).
- [16] S. Hikami, A.I. Larkin, Y. Nagaoka, *Prog. Theor. Phys.* **63**, 707 (1980).
- [17] A. Mackinnon, B. Kramer, *Phys. Rev. Lett.* **47**, 1546 (1981).
- [18] S.N. Evangelou, *Phys. Rev. Lett.* **75**, 2550 (1995).
- [19] Y. Asada, K. Slevin, T. Ohtsuki, *Phys. Rev. Lett.* **89**, 256601 (2002).
- [20] A. Mackinnon, B. Kramer, *Z. Phys. B Condens. Matter* **53**, 1 (1983).
- [21] J. Kosterlitz, *J. Phys. C Solid State Phys.* **7**, 1046 (1974).
- [22] T. Čadež, R. Mondaini, P.D. Sacramento, *Phys. Rev. B* **96**, 144301 (2017).
- [23] L. D'Alessio, A. Polkovnikov, *Ann. Phys.* **333**, 19 (2013).
- [24] M.Z. Hasan, C.L. Kane, *Rev. Mod. Phys.* **82**, 3045, (2010).
- [25] X.L. Qi, S.C. Zhang, *Rev. Mod. Phys.* **83**, 1057 (2011).
- [26] D.J. Thouless, M. Kohmoto, M.P. Nightingale, M. den Nijs, *Phys. Rev. Lett.* **49**, 405 (1982).
- [27] S. Nadj-Perge, I.K. Drozdov, B.A. Bernevig, A. Yazdani, *Phys. Rev. B* **88**, 020407, (2013).
- [28] J. Klinovaja, P. Stano, A. Yazdani, D. Loss, *Phys. Rev. Lett.* **111**, 186805, (2013).
- [29] S. Nadj-Perge, I.K. Drozdov, J. Li, H. Chen, S. Jeon, J. Seo, A.H. MacDonald, B.A. Bernevig, A. Yazdani, *Science* **346**, 602 (2014).
- [30] J. Alicea, *Rep. Prog. Phys.* **75**, 076501, (2012).
- [31] T.P. Choy, J.M. Edge, A.R. Akhmerov, C.W.J. Beenakker, *Phys. Rev. B* **84**, 195442 (2011).
- [32] M. Kjaergaard, K. Wölms, K. Flensberg, *Phys. Rev. B* **85**, 020503 (2012).
- [33] I. Martin, A.F. Morpurgo, *Phys. Rev. B* **85**, 144505 (2012).
- [34] S. Nakosai, Y. Tanaka, N. Nagaosa, *Phys. Rev. B* **88**, 180503 (2013).
- [35] B. Braunecker, P. Simon, *Phys. Rev. Lett.* **111**, 147202 (2013).
- [36] M.M. Vazifeh, M. Franz, *Phys. Rev. Lett.* **111**, 206802 (2013).
- [37] F. Pientka, L.I. Glazman, F.V. Oppen, *Phys. Rev. B* **88**, 155420 (2013).
- [38] F. Pientka, L.I. Glazman, F.V. Oppen, *Phys. Rev. B* **89**, 180505 (2014).
- [39] K. Pöyhönen, A. Westström, J. Röntynen, T. Ojanen, *Phys. Rev. B* **89**, 115109 (2014).
- [40] J. Röntynen, T. Ojanen, *Phys. Rev. B* **90**, 180503 (2014).
- [41] I. Reis, D.J.J. Marchand, M. Franz, *Phys. Rev. B* **90**, 085124 (2014).
- [42] Y. Kim, M. Cheng, B. Bauer, R.M. Lutchyn, S. Das Sarma, *Phys. Rev. B* **90**, 060401 (2014).
- [43] J. Li, T. Neupert, A. Bernevig, A. Yazdani, *Nat. Commun.* **7**, 10395 (2016).
- [44] A. Heimes, P. Kotetes, G. Schön, *Phys. Rev. B* **90**, 060507 (2014).
- [45] A. Heimes, D. Mendler, P. Kotetes, *New. J. Phys.* **17**, 023051 (2015).
- [46] Y. Peng, F. Pientka, L.I. Glazman, F.V. Oppen, *Phys. Rev. Lett.* **114**, 106801, (2015).
- [47] J. Li, H. Chen, I.K. Drozdov, A. Yazdani, A. Bernevig, A.H. MacDonald, *Phys. Rev. B* **90**, 235433 (2014).
- [48] P.M.R. Brydon, S.D. Sarma, H.Y. Hui, J.D. Sau, *Phys. Rev. B* **91**, 064505 (2015).

- [49] H.Y. Hui, P.M.R. Brydon, J.D. Sau, S. Tewari, S.D. Sarma, *Sci. Rep.* **5**, 8880 (2015).
- [50] K. Pöyhönen, A. Westström, T. Ojanen, *Phys. Rev. B* **93**, 014517 (2016).
- [51] T. Čadež, P.D. Sacramento, *J. Phys. Condens. Matter* **28**, 495703 (2016).
- [52] J. Rötynen, T. Ojanen, *Phys. Rev. Lett.* **114**, 236803 (2015).
- [53] Jian Li, T. Neupert, Z.J. Wang, A.H. MacDonald, A. Yazdani, B.A. Bernevig, *Nat. Comm.* **7**, 12297 (2016).
- [54] J. Rötynen, T. Ojanen, *Phys. Rev. B* **93**, 094521 (2016).
- [55] A. Westström, K. Pöyhönen, T. Ojanen, *Phys. Rev. B* **94**, 104519 (2016).
- [56] B. Roy, Y. Alavirad, J.D. Sau, *Phys. Rev. Lett.* **118**, 227002 (2017).
- [57] A.A. Abrikosov, L.P. Gor'kov, *Sov. Phys. JETP* **12**, 1243 (1961).
- [58] P.D. Sacramento, V. Dugaev, V.R. Vieira, M.A.N. Araújo, *J. Phys. Condens. Matter* **22**, 025701 (2010).
- [59] N. Read, D. Green, *Phys. Rev. B* **61**, 10267 (2000).
- [60] D.A. Ivanov, *Phys. Rev. Lett.* **86**, 268 (2001).
- [61] M. Sato, S. Fujimoto, *Phys. Rev. B* **79**, 094504 (2009).
- [62] P.D. Sacramento, *J. Phys. Condens. Matter* **27**, 445702 (2015).
- [63] K. Pöyhönen, I. Sahlberg, A. Westström, T. Ojanen, *Nat. Comm.* **9**, 2103 (2018).
- [64] A.V. Balatsky, I. Vekhter, J.X. Zhu, *Rev. Mod. Phys.* **78**, 373 (2006).
- [65] L. Yu, *Acta Phys. Sin.* **21**, 75 (1965).
- [66] H. Shiba, *Prog. Theor. Phys.* **40**, 435 (1968).
- [67] A. Rusinov, *Sov. Phys. JETP* **29**, 1101 (1969).
- [68] A. Sakurai, *Prog. Theor. Phys.* **44**, 1472 (1970).
- [69] M.I. Salkola, A.V. Balatsky, J.R. Schrieffer, *Phys. Rev. B* **55**, 12648 (1997).
- [70] M.E. Flatté, J.M. Byers, *Phys. Rev. Lett.* **78**, 3761 (1997).
- [71] A. Yazdani, B.A. Jones, C.P. Lutz, M.F. Crommie, D.M. Eigler, *Science* **275**, 1767 (1997).
- [72] S.H. Ji, T. Zhang, Y.S. Fu, X. Chen, X.C. Ma, J. Li, W.H. Duan, J.F. Jia, Q.K. Xue, *Phys. Rev. Lett.* **100**, 226801 (2008).
- [73] N. Hatter, B.W. Heinrich, M. Ruby, J.I. Pascual, K.J. Franke, *Nat. Commun.* **6**, 8988 (2015).
- [74] A.P. Schnyder, S. Ryu, A. Furusaki, A.W.W. Ludwig, *Phys. Rev. B* **78**, 195125 (2008).
- [75] T. Fukui, Y. Hatsugai, H. Suzuki, *J. Phys. Soc. Jpn.* **74**, 1674 (2005).
- [76] Y.F. Zhang, Y.Y. Yang, Y. Ju, L. Sheng, R. Shen, D.N. Sheng, D.Y. Xing, *Chin. Phys. B* **22**, 117312 (2013).
- [77] J. Lages, P.D. Sacramento, Z. Tešanović, *Phys. Rev. B* **69**, 094503 (2004).
- [78] A. Mildemberger, F. Evers, A.D. Mirlin, J.T. Chalker, *Phys. Rev. B* **75**, 245321 (2007).
- [79] I.C. Fulga, A.R. Akhmerov, J. Tworzydło, B. Béri, C.W.J. Beenakker, *Phys. Rev. B* **86**, 054505 (2012).
- [80] A.Y. Kitaev, *Phys. Usp.* **44**, 131, (2001).
- [81] T. Čadež, R. Mondaini, P.D. Sacramento, *Phys. Rev. B* **99**, 014301 (2019).
- [82] O. Balabanov, H. Johannesson, *Phys. Rev. B* **96**, 035149 (2017).
- [83] M.T. Rieder, L.M. Sieberer, M.H. Fischer, I.C. Fulga, *Phys. Rev. Lett.* **120**, 216801 (2018).
- [84] L.M. Sieberer, M.T. Rieder, M.H. Fischer, I.C. Fulga, *Phys. Rev. B* **98**, 214301 (2018).